References

[1] Athans, M. and Falb, P. L., *Optimal Control: An Introduction to the Theory and Its Applications*, McGraw-Hill, New York, 1966.

[2] Robbins, H. M., "A Generalized Legendre-Clebsch Condition for the Singular Cases of Optimal Control," *IBM Journal of Research and Development*, Vol. 11, No. 4, July 1967, pp. 361–372.

[3] Kelley, H. J., Kopp, R. E., and Moyer, H. G., "Singular Extremals," *Topics in Optimization*, edited by G. Leitmann, Academic Press, New York, 1967, pp. 63–101.

[4] Anderson, G. M., "Necessary Conditions for Singular Solutions in Differential Games with Controls Appearing Linearly," *Proceedings of the First International Conference on the Theory and Application of Differential Games*, Automatic Control Group of the Institute of Electrical and Electronics Engineers, Amherst, Mass., Oct. 1969.

[5] McDanell, J. P. and Powers, W. F., "New Jacobi-Type Necessary and Sufficient Conditions for Singular Optimization Problems," *AIAA Journal*, Vol. 8, No. 8, Aug. 1970, pp. 1416–1420.

[6] Jacobson, D. H. and Speyer, J. L., "Necessary and Sufficient Conditions for Optimality for Singular Control Problems: A Limit Approach," TR-604, March 1970, Div. of Engineering and Applied Physics, Harvard Univ., Cambridge, Mass.; also *Journal of Mathematical Analysis and Applications*, to be published.

[7] Speyer, J. L. and Jacobson, D. H., "Necessary and Sufficient Conditions for Optimality for Singular Control Problems: A Transformation Approach," *Journal of Mathematical Analysis and Applications*, Vol. 33, No. 1, Jan. 1971, pp. 163–187.

[8] Jacobson, D. H., "On Singular Arcs and Surfaces in a Class of Quadratic Minimization Problems," TR 613, Aug. 1970, Div. of Engineering and Applied Physics, Harvard Univ., Cambridge, Mass.; also *Journal of Mathematical Analysis and Applications*, to be published.

JULY 1971 J. SPACECRAFT VOL. 8, NO. 7

A Jupiter Orbiter Mechanics Experiment

CHARLES K. PAUL*
Cornell University, Ithaca, N.Y.

An X-band radar onboard a planetary orbiting spacecraft measuring range and range rate to the planetary surface is not only capable of refining spacecraft orbit determination, but can also be employed to map the planet's gravitational potential. The number of gravitational harmonic coefficients which can be solved is dependent upon the radar accuracy in measuring range rate. In the case of a Jupiter orbiter, spacecraft propulsion penalties and science objectives favor highly eccentric equatorial orbits in which the spacecraft is within radar-measuring range of the planet for only a few hours of the long 40-day period. The radar orbit determination scheme formulated here is thus a short-arc method and the short-term periodic perturbations to the orbit caused by the planet's potential are significant during this close approach phase to the planet. These perturbations on the equatorial orbital elements are derived and expressed as terms of the measured range rate. The theoretical formulation is termed the range rate model and allows solution of four of Jupiter's harmonic coefficients. The only significant nonplanetary perturbations to the measured range rates are caused by Jupiter's closest five natural satellites. The formulation necessary to correct range rates for these perturbations is developed.

Introduction

MAJOR planetary orbiters starting with Jupiter in the early 1980's are logical follow-ups to the late 1970 Grand Tour missions. An orbiter is ideal for studying planetary mass and gravitational properties affecting the spacecraft orbit. The spacecraft utilizes onboard instrumentation provided for other mission objectives, thus no weight or power penalties are associated with this type of experiment.

The theory of satellite geodesy for analyzing the Earth's potential has been well summarized during the past decade.[1] The orbits of geodetic satellites can generally be described as nearly circular with periods of about $1\frac{1}{2}$ hr, the satellite orbiting within one Earth radius of the planet's surface and hence being significantly perturbed by higher order terms of the gravitational potential throughout its orbit. As opposed to terrestrial orbiters, propellant requirements and science objectives dictate highly eccentric orbits about the major planets; e.g., for Jupiter, a 1.1 Jupiter radius (R_J) perijove by 100 R_J apojove orbit is suggested.[2] The orbital period is 45 days and the spacecraft is within $1\frac{1}{2}$ Jupiter radii of the planet's surface for only 2 hr during each orbit. This short duration in the proximity of the planet and the fact that a certain degree of hydrostatic equilibrium suggested by present planetary models of Jupiter[3,4] imply a rapid diminution of the higher order gravity harmonics. Thus only the central term and the second and fourth degree zonals ($J_2 = 0.01470$, $J_4 = -0.00067$)[3,5] of the potential were used to calculate the secular perturbations on various Jupiter orbits.[6] The small secular rates of motion,[6] orbital trim to satisfy science objectives, and secondary perturbational effects during the long duration at apojove caused by other celestial body gravitational fields, solar radiation pressure, propellant tank leakage, and downlink telemetry maneuvers all combine to eliminate the secular and long term orbital rates over an integral number of orbits as a means for zenodetic analysis. Thus direct observation of the short-term periodic effects is predicated. Observation capability implies onboard navigation capabilities in the form of the existing radio transmitter and receiver, the imaging system, and the X-band radar. Deep Space Network (DSN) tracking alone will not suffice when the long $1\frac{1}{2}$ hr radio round trip time, DSN scheduling, and spacecraft perijove occultations from Earth are considered. Figure 1 shows the 1.1 by 100 R_J orbit.

Received September 1, 1970; revision received January 12, 1971. The author wishes to acknowledge the support of NASA under contract NGR 33-010-071 which made possible a large portion of this research.

* Professor of Engineering.

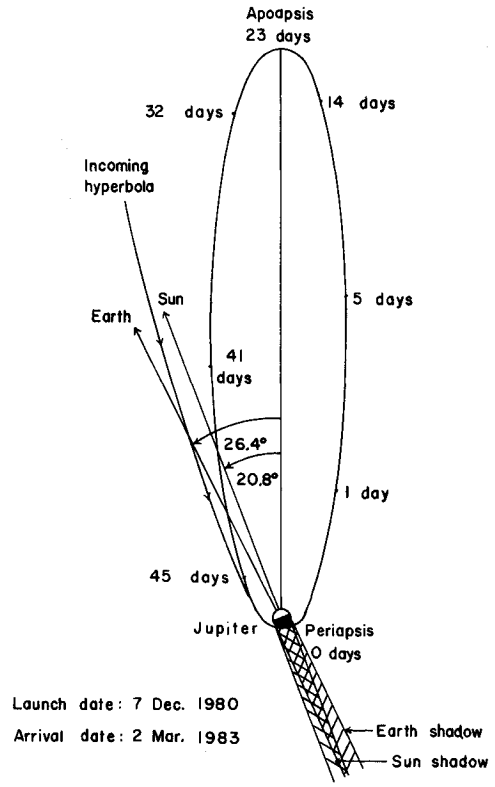

Fig. 1 Geometry of Jupiter 1.1 R_J × 100 R_J spacecraft orbit.

The question of X-band radar reflections from Jupiter's atmosphere is discussed under Conclusions.

Formulation of the Short-Term Periodic Perturbations to an Equatorial Orbit

The potential model adopted for Jupiter's gravitational potential is expressed

$$V = \frac{GM_J}{r} - \frac{GM_JR_J^2J_2}{r^3}P_2(\sin\phi) - \frac{GM_JR_J^4J_4}{r^5} \times P_4(\sin\phi) - \frac{GM_JR_J^2}{r^3}P_{22}(\sin\phi)(C_{22}\cos 2\lambda + S_{22}\sin 2\lambda) \quad (1)$$

where V is the potential due to Jupiter's gravitation in units of velocity squared on a unit mass with zenocentric coordinates (r,ϕ,λ) defining distance, latitude, and longitude respectively; GM_J is Jupiter's gravitational mass = 1.267077 × 10^8 km^3/sec^2 (Refs. 3 and 4); R_J is Jupiter's equatorial radius = 71,372 km (Refs. 3 and 4); J_n, C_{nm}, and S_{nm} are harmonic coefficients; and P_{nm} are the Associated Legendre polynomials, degree n, order m (the zonals $m = 0$ are written as P_n).

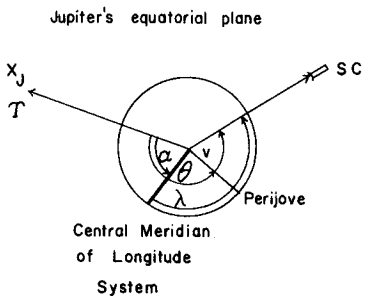

Fig. 2 Equatorial relation between spacecraft true anomaly v and longitude λ.

The Lagrange equations modified in Ref. 6 (Appendix C) applicable for the perturbations on a spacecraft equatorially orbiting a planetary body are

$$da/dt = (2/na)\partial F/\partial M$$
$$de/dt = [(1-e^2)/na^2e]\partial F/\partial M - [(1-e^2)^{1/2}/na^2e]\partial F/\partial\Theta \quad (2)$$
$$dM/dt = (-2/na)\partial F/\partial a - [(1-e^2)/na^2e]\partial F/\partial e$$
$$d\Theta/dt = [(1-e^2)^{1/2}/na^2e]\partial F/\partial e$$

where a is the orbit semimajor axis, n the mean orbital velocity given by $(GM_J/a^3)^{1/2}$, e the eccentricity, Θ the right ascension of perijove, M the mean anomaly, and F the force function equal to the difference between gravitational and kinetic energies; i.e.,

$$F = V - \tfrac{1}{2}v^2 \quad (3)$$

where v is the spacecraft zenocentric orbital velocity

$$v = [GM_J(2/r - 1/a)]^{1/2} \quad (4)$$

Figure 2 relates the longitude λ to the true anomaly v for an equatorial orbit; i.e.,

$$\lambda = \Theta - \alpha + v \quad (5)$$

where α is the right ascension of the System I or III† central meridian. The zenocentric axes $(\mathbf{X}_J,\mathbf{Y}_J,\mathbf{Z}_J)$, $\mathbf{X}_J$ the equatorial projection of the Aries vector, $\mathbf{Z}_J$ the north polar axis, are formulated in Ref. 6 (p. 173).

A careful secular perturbational analysis in Ref. 6 as well as the fact that Jupiter's Galilean satellites are nearly equatorial confirms the assumption of orbital equatorial stability. Thus, evaluating the Legendre polynomials at zero and using Eqs. (1 and 3–5), the force function becomes

$$F = GM_J/2a + GM_JR_J^2\{J_2/2r^3 - (3R_J^2J_4/8r^5) - (3/r^3)[C_{22}\cos 2(\Theta - \alpha + v) + S_{22}\sin 2(\Theta - \alpha + v)]\} \quad (6)$$

Using the following well-known equations of orbital mechanics

$$r = a(1-e^2)/(1 + e\cos v) \quad (7)$$
$$dr/dv = re\sin v/(1 + e\cos v) \quad (8)$$
$$dv/dM = a^2(1+e^2)^{1/2}/r^2 \quad (9)$$

the substitution of Eq. (6) into Eq. (2) yields the short-term periodic perturbations in terms of the assumed unknown coefficients

$$\begin{pmatrix} da/dt \\ de/dt \\ dM/dt \\ d\Theta/dt \end{pmatrix} = \begin{pmatrix} 0 \\ 0 \\ n \\ 0 \end{pmatrix} + \mathbf{G}\begin{pmatrix} J_2 \\ J_4 \\ C_{22} \\ S_{22} \end{pmatrix} \quad (10)$$

where G is the 4 by 4 matrix $\{g_{ij}(r,a,e,v,\Theta)\}$. The individual g_{ij} are derived in Appendix E of Ref. 6 and are not presented here.

Solution of the Gravitational Harmonic Coefficients with the Onboard Radar

Figure 3 indicates several of the general points along the 1.1 R_J by 100 R_J Jupiter euqatorial orbit at which radar range and range-rate measurements are made. Assuming a radar

† Jupiter's Systems I and III longitude systems are based on equatorial atmospheric and decametric phenomena, respectively.

reflection at a distance of δR_J,‡ the radar range and range-rate measurements yield:

$$r = R + \delta R_J, \quad \dot{r} = c\Delta f_i/f_i \tag{11}$$

where R is the radar range to Jupiter's atmosphere, c is the velocity of electromagnetic radiation through Jupiter's ionosphere, f_i is the X-band frequency of the signal, and Δf_i is the measured frequency shift due to the Doppler effect caused by $\dot{r}$ of the spacecraft.

Preliminary analysis[2] indicates that range accuracies of from ten to twenty kilometers and range-rate accuracies of from 10 to 20 m/sec are possible with an X-band radar at Jupiter distances of from 1.1 to 2.5 R_J. These accuracies assume that range and range-rate measurements have been corrected for ionospheric and tropospheric refraction effects, as well as errors in the reference frequency f_i and radar failure to lock onto the signal. They do not take into account errors caused by radio propagation times nor atmospheric attenuation effects.

Equation (7) is the basis for the range rate model. If the equatorial spacecraft orbit about Jupiter were strictly Keplerian; i.e., the central gravity term only were present; $\dot{r}$ would be strictly a function of the true anomaly v, or of the spacecraft position in an orbit of constant semimajor axis a and eccentricity e. However, the smaller remaining terms of the potential affect $\dot{r}$ through the periodic perturbations to a, e, and v derived above. But these perturbations have been expressed explicitly in terms of the unknown harmonic coefficients in Eq. (10). Thus, by measuring $\dot{r}$ accurately, and providing that the osculating values of (a,e,v,Θ) can be solved, a solution for the unknown harmonics can be affected.

Using Eqs. (7) and (9), the range rate model is expressed as

$$\dot{r} = \frac{r}{a}\frac{da}{dt} - \frac{r[2e + (1 + e^2)\cos v]}{(1 - e^2)(1 + e\cos v)}\frac{de}{dt} + \frac{a^2 e \sin v}{r}\frac{(1 - e^2)^{1/2}}{1 + e\cos v}\frac{dM}{dt} \tag{12}$$

Substitution of Eq. (10) into Eq. (12) and considering all observation points 1 through n, the following vector of range rates is derived

$$\dot{\mathbf{r}} = \mathbf{AJ} + \mathbf{E} \tag{13}$$

where $\dot{\mathbf{r}}$ is the $n \times 1$ column vector $\{\dot{r}_i\}$ of range rates for all positions 1 through n, $\mathbf{A}$ is the $n \times 4$ matrix $\{a_{ij}\}$, $\mathbf{J}^T$ is the 1×4 row vector $(J_2, J_4, C_{22}, S_{22})$ of unknown coefficients, $\mathbf{E}$ is the $n \times 1$ column vector $\{E_i\}$, where

$$E_i = n_i a_i e_i \sin v_i/(1 - e_i^2)^{1/2}$$

The functions $\{a_{ij}(r_i,a_i,e_i,v_i,\Theta_i)\}$ are given in Ref. 6.

$\mathbf{J}$ can thus be solved by the usual methods of vector algebra once the osculating values of (a_i,e_i,v_i,Θ_i) are determined for each position i, as described below. If n is greater than 4, a least-squares solution for $\mathbf{J}$ is suggested. It should also be noted that Eq. (13) is well conditioned for observations taken along the orbit where: $-\pi/2 \leq v \leq \pi/2$, as $\dot{r}$, a, and E vary considerably along this orbital arc.

A Short Arc Orbit Determination Scheme

Condition Equations

The successful implementation of the range-rate model requires the knowledge of the osculating orbital parameters at each radar measurement point i, $i = 1,\ldots,n$. These parameters can be obtained at each point by means of the R and RR observations and two additional measurements; i.e., (1) the precise timing of each radar measurement so that the time interval $\Delta t_{k+1,k}$ between the k + 1st and the kth measurement can be determined, and (2) one or more radar measurements of Jupiter's natural satellite JV (Amalthea). Measurements (1) require a very preciseon board timing reference normally incorporated within the data automation systems of interplanetary spacecraft. Measurements (2) obtain range and range-rate data from Jupiter's closest natural satellite as simultaneously as possible with one pair of similar data from the planet.

‡ δR_J will be close to one R_J. A probable radar reflection surface would be Jupiter's cloudtop boundary marking the equilibrium point of vapor and solid phases of ammonia at about 20–40 km below Jupiter's tropopause,[3] a distance compatible to the radar-range accuracy.

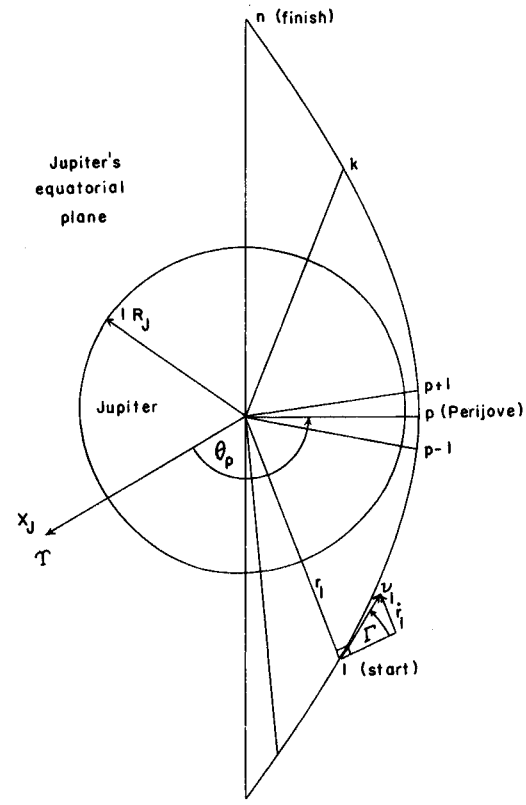

Fig. 3 Radar range and range-rate measurements to Jupiter's atmosphere.

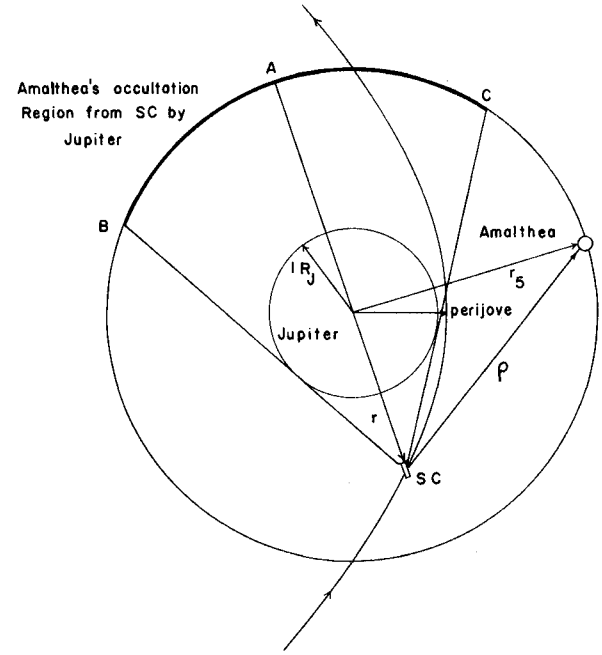

Fig. 4 Spacecraft-Amalthea orbital characteristics.

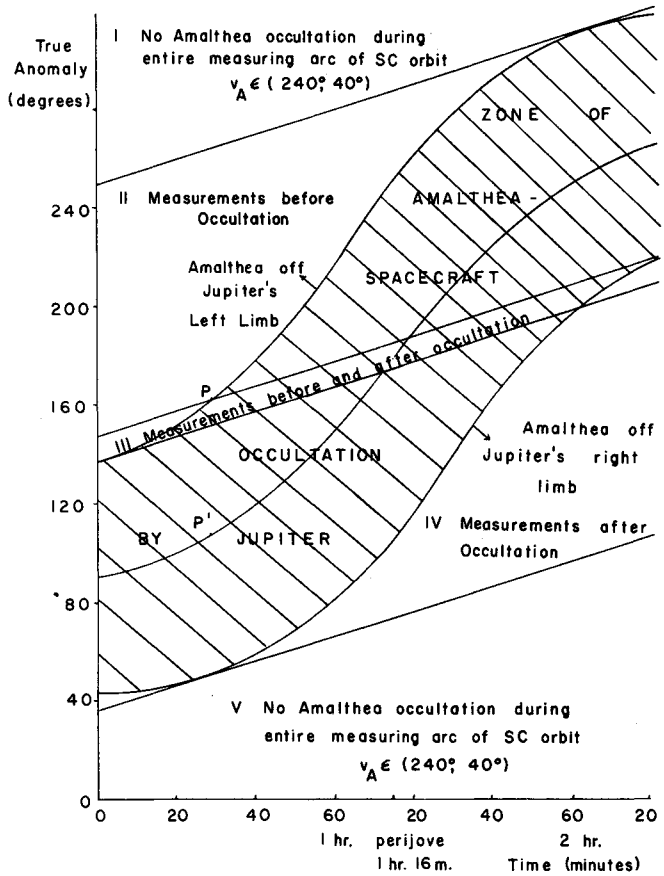

Fig. 5 Region of Amalthea occultation.

In addition, any science imaging along this arc of radar measurements revealing celestial body configurations such as Jupiter limb, natural satellites, planets, and stars can likewise be utilized for orbit determination refinement. All orbital measurements, including planetary and satellite R and RR, times of observations, and imaging data are encoded and later telemetered to Earth after the spacecraft has proceeded past point n. Because of spacecraft weight restrictions eliminating a sophisticated onboard processing unit, the orbit determination and gravity mapping analyses are performed on Earth.

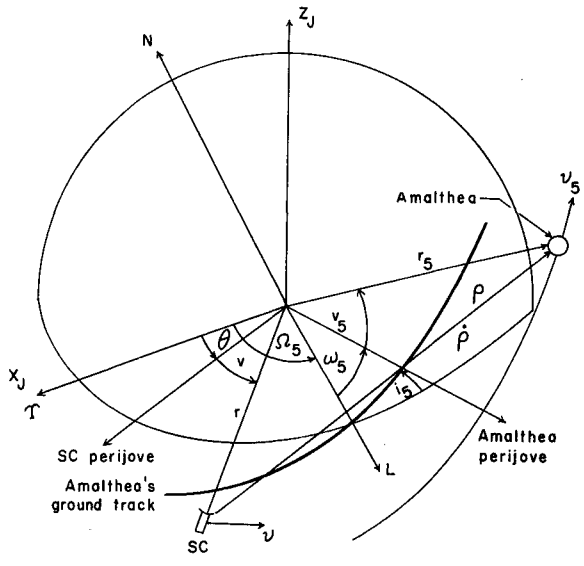

Fig. 6 Reduction of Spacecraft-Amalthea radar data.

The short-arc solution takes advantage of one condition at each planetary measurement point i and a second condition involving points $i - 1$ and i. The first anomaly condition involves the osculating true anomaly v. The second Lambert condition involves the direct solution of Kepler's equation between points $i - 1$ and i. Kepler's equation solves for the time required to travel between 2 points on an ellipse given the radial distances of the points from the central attracting body and the semimajor axis of the ellipse. Since time is very precisely monitored on the spacecraft, direct solution of Kepler's equation is desirable.

The anomaly condition is formulated first. For any observation point i of Fig. 3, the path angle Γ can be expressed

$$\sin\Gamma = [r/(1 - e^2)(2a - r)]^{1/2} e \sin v \tag{14}$$

where $0 \leq \Gamma \leq \pi/2$ if $0 \leq v \leq \pi$; $-\pi/2 \leq \Gamma \leq 0$ if $\pi \leq v \leq 2\pi$.

Again, from Fig. 3

$$\dot{r} = v \sin\Gamma \tag{15}$$

substituting for v from Eq. (4) and using Eqs. (14) and (15):

$$\sin v = [a(1 - e^2)/GM_J]^{1/2} \dot{r}/e \tag{16}$$

Using Eqs. (7) and (11):

$$\cos v = (1/e)[a(1 - e^2)/r - 1] \tag{17}$$

Equations (16) and (17), and the identity $\sin^2 v + \cos^2 v = 1$ yield an equation involving 2 unknowns (a,e) and 2 measured quantities $(R,\dot{r})$. If the true osculating values of (a,e) were known and substituted into this equation, a functional expression could be written

$$F_1(a,e) = 0 \tag{18}$$

where

$$F_1(a,e) = a^2(1 - e^2)^2/r^2 + (\dot{r}^2/GM_J - 2/r)a(1 - e^2) + 1 - e^2$$

If appropriate values (a^0,e^0) for the true orbital elements are substituted into Eq. (18), F_1 will not equal zero, and the corrections $(\Delta a, \Delta e)$ to the approximate values can be developed through the Taylor series approximation of (18); i.e.,

$$(\partial F_1/\partial a)\Delta a + (\partial F_1/\partial e)\Delta e = -F_1(a^0,e^0) \tag{19}$$

$F_1, \partial F_1/\partial a$, and $\partial F_1/\partial e$ are evaluated at $(a,^0e^0)$.

The Lambert condition begins with equation Eq. (17) for points $i - 1$ and i, thus v_{i-1} and v_i are expressed in terms of $(a_{i-1},e_{i-1},r_{i-1})$ and (a_i,e_i,r_i) respectively. The eccentric anomaly at each point is defined

$$\cos E_i = (e_i + \cos v_i)/(1 + e_i \cos v_i) \tag{20}$$

For this special case of an orbital arc between $v = -\pi/2$ and $\pi/2$, E_i will always be in the same quadrant as v_i.

The mean anomaly at each point is defined

$$M_i = E_i - e_i \sin E_i \tag{21}$$

Thus the mean anomaly difference between points $i - 1$ and i is simply

$$\Delta M = (E_i - E_{i-1}) - (e_i \sin E_i - e_{i-1} \sin E_{i-1}) \tag{22}$$

The time required to travel between the two points is very nearly:

$$t = F_2(a,e) = (a^3/GM_J)^{1/2} \Delta M \tag{23}$$

providing the time interval $\Delta t_{i,i-1}$ is maintained short enough (less than 5 min) such that a linear average semimajor axis can be substituted for a in Eq. (23). This implies that the osculating semimajor axis is being approximated by a straight line between the points $i - 1$ and i.

The Lambert condition then merely equates this computed time to the measured time interval; i.e., if the true values of (a,e) at both points were known and the measured time interval is corrected for all systematic errors, then

$$[F_2(a,e) - \Delta t]_{i,i-1} = 0 \tag{24}$$

Letting

$$F_{2i}(a_i,r_i,e_i) = \cos^{-1}[(a_i - r_i)/a_ie_i] - (1/a_i)[-a_i^2(1 - e_i^2) + 2a_ir_i - r_i^2]^{1/2}$$

then

$$F_2(a_i,e_i) = \{[(a_i + a_{i-1})^3]/8GM_J\}^{1/2}(F_{2i} - F_{2,i-1})$$

For reasons to be discussed shortly, the values of (a_{i-1},e_{i-1}) are assumed known. Then the failure of equality in Eq. (24) is due to errors in approximating (a_i,e_i). If corrections to these parameters are designated $(\Delta a_i,\Delta e_i)$, then the following equation is valid combining Eqs. (17 and 20–24); and expanding Eq. (24) into its Taylor series

$$(\partial F_2/\partial a_i)\Delta a_i + (\partial F_2/\partial e_i)\Delta e_i = -[F_2(a_i^0,e_i^0) - \Delta t_{i,i-1}] \tag{25}$$

$\partial F_2/\partial a_i$, $\partial F_2/\partial e_i$, and F_2 are all evaluated with the approximate values (a_i^0,e_i^0).

Thus, considering the point i, Eqs. (19) and (25) allow solution of the two unknowns; i.e., Δa_i and Δe_i. These values are added respectively to a_i^0 and e_i^0 and Eqs. (19) and (25) are iterated until the corrections Δa_i and Δe_i become less than some stipulated values. Thus, using $i - 1$ as a starting point, the solution can be stepped foreward in this manner to point n and backward to point 1. The determination of an initial orbital set (a_{i-1},e_{i-1}) is described in the following section. The true anomaly v at each point is solved from Eq. (17).

The advantage of this double condition solution is that only 2×2 matrices need be inverted, suggesting that a certain amount of onboard processing of navigational data is possible. There is also no need for a large number of computations which would be required in a simple differential-correction scheme since the small term periodic perturbations Eq. (10) are of large magnitude.

JV (Amalthea) Radar Measurements

Figure 4 reveals the geometry between the orbits of the spacecraft and Amalthea. Amalthea's orbit is very nearly circular, as seen in Table 1.

Figure 5 is the Amalthea-spacecraft occultation region. The ordinate axis plots true anomaly referenced to the spacecraft perijove, which the spacecraft reaches one hour and sixteen minutes after entering the radar measuring arc ($v = -\pi/2$) at time zero as indicated on the abscissa axis. The occultation region is shown as the locus of intersection of a cone with the spacecraft as vertex, subtended angle of Jupiter as vertex angle, and Amalthea's orbital ellipse. The ordinate width of the occultation zone defines the base diameter of the

Table 1 Orbital elements of Jupiter's closest five satellites[4]

Satellite	Semimajor axis, km	Eccentricity	Inclination (to Jupiter's equator), deg-min	Sidereal period, d- h-m- s
JV (Amalthea)	181,500	0.0028	0 27.3	0-11-57-22.70
JI (Io)	422,000	0.0000	0 01.6	1-18-27-33.51
JII (Europa)	671,400	0.0003	0 28.1	3-13-13-42.05
JIII (Ganymede)	1,071,000	0.0015	0 11.0	7-03-42-33.35
JIV (Callisto)	1,884,000	0.0075	0 15.2	16-16-32-11.21

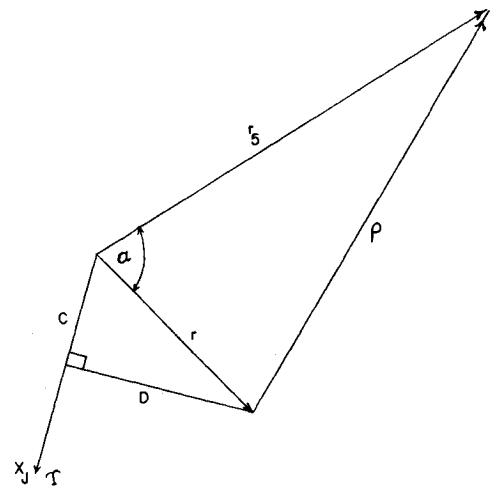

Fig. 7 Vector representation of the spacecraft zenocentric distance.

cone at Amalthea's orbit intersection. The true anomaly of the spacecraft is 180° plus or minus the anomaly of the center line of the occultation region. Since Amalthea's orbital velocity is nearly constant, its true anomaly as a function of time plots as a straight line.

The 5 regions of occultation characteristics are shown in Fig. 5. In real time, as the spacecraft enters the radar-measuring arc and with a value of Amalthea's anomaly obtained from ephemerides, times available for Amalthea radar measurements outside of the crosshatched occultation zone are thus known. From all of the available spacecraft points, that point lying simultaneously closest to the center line of the occultation zone $(P - P')$ is the most desirable for it minimizes the turning angle required in pointing the spacecraft radar antenna alternately from Jupiter to Amalthea. It is thus seen from Fig. 5 that it is always possible to radar range and range rate on Amalthea during the radar-measuring arc of the spacecraft orbit. The worst visibility condition occurs in the region marked III of Fig. 5, although an initial true anomaly for Amalthea of 150° still permits 20 min of satellite measurements.

Assuming the orbital parameters of Amalthea are known at any time§ $(a_5,e_5,v_5,\ i_5,\omega_5,\Omega_5)$; where v_5 is Amalthea's true

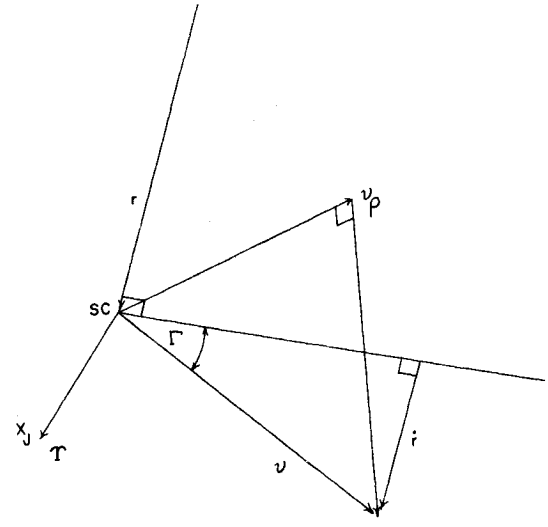

Fig. 8 Solution for the spacecraft velocity vector.

§ Jupiter satellite orbital improvements can be expected from 1970 Pioneers F and G and Grand Tour missions.

anomaly with respect to Amalthea's perijove, i_5 is the inclination, ω_5 is the argument of perijove, Ω_5 is the right ascension of the ascending node, and the subscript 5 represents Amalthea (JV); and consulting Fig. 4, the zenocentric range (r_5), linear velocity (v_5), and path angle (Γ_5) for Amalthea are given by Eqs. (7, 4, and 14), respectively, with all variables having the subscript 5.

The planetary radar measurement provides r and $\dot{r}$ while Amalthea radar-range and range-rate measurements provide ρ and $\dot{\rho}$, respectively. The problem is to determine the spacecraft's orbital semimajor axis from this data. The solution is determined by finding the spacecraft's linear velocity v and using Eq. (4). Although the zenocentric range (r) of the spacecraft is known, the first step is to determine the vector representation ($\mathbf{r}$) for this distance.

The zenocentric axes ($\mathbf{X}_J$,$\mathbf{Y}_J$,$\mathbf{Z}_J$) are used as a basis. These vectors were introduced after Eq. (5); however, they can be zenocentrically localized for this derivation as: $\mathbf{X}_J = (1,0,0)$, $\mathbf{Y}_J = (0,1,0)$, $\mathbf{Z}_J = (0,0,1)$.

Orthonormal vectors defining Amalthea's orbital plane are developed by formulating the unit vector $\mathbf{L}$ through Amalthea's ascending node (see Fig. 6)

$$\mathbf{L} = \cos\Omega_5\mathbf{X}_J + \sin\Omega_5\mathbf{Y}_J \tag{26}$$

The normal unit vector $\mathbf{N}$ to Amalthea's orbital plane is

$$\mathbf{N} = \sin i_5 \sin\Omega_5\mathbf{X}_J - \sin i_5 \cos\Omega_5\mathbf{Y}_J + \cos i_5\mathbf{Z}_J \tag{27}$$

$$\mathbf{M} = \mathbf{N} \times \mathbf{L} \tag{28}$$

completes this orthonormal system. The vector representation of Amalthea's zenocentric distance is

$$\mathbf{r}_5 = r_5[\cos(\omega_5 + v_5)\mathbf{L} + \sin(\omega_5 + v_5)\mathbf{M}] \tag{29}$$

Amalthea's velocity vector is then

$$\mathbf{v}_5 = (v_5/r_5)[(\mathbf{N} \times \mathbf{r}_5)\cos\Gamma_5 + \mathbf{r}_5 \sin\Gamma_5] \tag{30}$$

Use is now made of the triangle involving sides r, r_5, and ρ of Fig. 7. Since the vector representation for $r(\mathbf{r})$ in the basis ($\mathbf{X}_J$,$\mathbf{Y}_J$,$\mathbf{Z}_J$) will have a $\mathbf{Z}_J$ component equal to 0, $\mathbf{r}$ can be expressed as

$$\mathbf{r} = C\mathbf{X}_J + D\mathbf{Y}_J \tag{31}$$

where C and D are unknown values. Noting that the angle α is solved by the cosine law; i.e.,

$$\cos\alpha = (r_5^2 + r^2 - \rho^2)/2\rho r_5 \tag{32}$$

it is evident that

$$C(\mathbf{r}_5\cdot\mathbf{X}_J)/r_5 + D(\mathbf{r}_5\cdot\mathbf{Y}_J)/r_5 = r\cos\alpha \tag{33}$$

The condition that $(C^2 + D^2)^{1/2} = r$ allows the solution of C and D by the intersection of the straight line (33) and the circle of radius r. Although there are in fact two solutions, the desired solution can be immediately chosen by knowing whether the spacecraft is ahead or behind Amalthea in their respective orbits.

The vector of length ρ between the spacecraft and Amalthea is

$$\boldsymbol{\varrho} = \mathbf{r}_5 - \mathbf{r} \tag{34}$$

The component $(\mathbf{v}_5)_\rho$ along the direction $\boldsymbol{\varrho}$ is

$$(\mathbf{v}_5)_\rho = (\mathbf{v}_5\cdot\boldsymbol{\varrho})\boldsymbol{\varrho}/\rho \tag{35}$$

Thus the vector component $(\mathbf{v}_\rho)$ of the spacecraft velocity $\mathbf{v}$ along the direction $\boldsymbol{\varrho}$ is

$$\mathbf{v}_\rho = [(\mathbf{v}_5\cdot\boldsymbol{\varrho})/\rho - \dot{\rho}]\boldsymbol{\varrho} \tag{36}$$

Figure 8 indicates that the spacecraft velocity $\mathbf{v}$ is determined from $\mathbf{v}_\rho$ and $\dot{r}$, since $\dot{\mathbf{r}}$ is in the same or opposite direction as $\mathbf{r}$. Since $\mathbf{v}$ lies in Jupiter's equatorial plane, the velocity can be expressed

$$\mathbf{v} = A\mathbf{X}_J + B\mathbf{Y}_J \tag{37}$$

Since $\mathbf{v}_\rho$ is a projection of $\mathbf{v}$:

$$(\mathbf{v} - \mathbf{v}_\rho)\cdot\mathbf{v}_\rho = 0 \tag{38}$$

It is also noted from Fig. 8 and Eq. (15) that

$$\mathbf{v}\cdot\mathbf{r} = vr\sin\Gamma = r\dot{r} \tag{39}$$

Substituting Eq. (37) into Eqs. (38) and (39) yields two equations in two unknowns, A and B, the solutions are

$$A = \begin{vmatrix} v_\rho^2 & \mathbf{Y}_J\cdot\mathbf{v}_\rho \\ r\dot{r} & \mathbf{Y}_J\cdot\mathbf{r} \end{vmatrix} \Big/ \begin{vmatrix} \mathbf{X}_J\cdot\mathbf{v}_\rho & \mathbf{Y}_J\cdot\mathbf{v}_\rho \\ \mathbf{X}_J\cdot\mathbf{r} & \mathbf{Y}_J\cdot\mathbf{r} \end{vmatrix} \tag{40a}$$

$$B = \begin{vmatrix} \mathbf{X}_J\cdot\mathbf{v}_\rho & v_\rho^2 \\ \mathbf{X}_J\cdot\mathbf{r} & r\dot{r} \end{vmatrix} \Big/ \begin{vmatrix} \mathbf{X}_J\cdot\mathbf{v}_\rho & \mathbf{Y}_J\cdot\mathbf{v}_\rho \\ \mathbf{X}_J\cdot\mathbf{r} & \mathbf{Y}_J\cdot\mathbf{r} \end{vmatrix} \tag{40b}$$

Thus the vector and magnitude of the spacecraft velocity is determined and hence the semimajor axis a of the spacecraft orbit; i.e.,

$$a = rGM_J/(2GM_J - rv^2) \tag{41}$$

The spacecraft orbital eccentricity can now be solved from the anomaly condition Eq. (18) by substituting the semimajor axis a of Eq. (41) and zero for the Δa correction in Eq. (19) and iterating. The true anomaly v is found from Eq. (17) and the osculating right ascension of perijove Θ by noting that the zenocentric distance vector $\mathbf{r}$ can also be expressed as

$$\mathbf{r} = r\cos(\Theta + v)\mathbf{X}_J + r\sin(\Theta + v)\mathbf{Y}_J \tag{42}$$

Equating Eqs. (31) and (42)

$$\Theta = \tan^{-1}(D/C) - v \quad (C \neq 0) \tag{43}$$

Orbital Refinement

It is seen that the spacecraft orbit solution has two simplifications that would tend to degrade the accuracy of the solution for the gravitational harmonics. One assumption was that the time interval between successive planetary radar measurements was small enough such that a linear average semimajor axis could be used in Eq. (23). The second difficulty is noted that an osculating value of right ascension of perijove Θ can only be determined at the point where a natural satellite radar measurement is made [Eq. (43)]. Estimates of Θ for all of the other points have to be made for use in Eq. (13). It is pointed out that Θ appears only in the $\mathbf{A}$ matrix of Eq. (13).

The solved set of harmonic solutions $\mathbf{J}$ can be used to improve the accuracy of the orbital parameters (especially Θ) by rigorous integration of Eq. (10). Since the true anomaly v is changing much more rapidly than a, e, and Θ, the orbital rates Eq. (10) are considered as functions of v only from one point to the successive point. In terms of a, e, and Θ, the continuously changing functions Eq. (10) are being approximated by step functions. The improved orbital parameters (designated below with a superscript 1) at a point i are expressed in terms of the improved parameter at point $i - 1$ plus the integral of the change in the parameter as a function of v:

$$a_i^1 = a_{i-1}^1 + \int_{v_{i-1}}^{v_i} \frac{da}{dt}(v)\frac{dt}{dv}\,dv \tag{44a}$$

$$e_i^1 = e_{i-1}^1 + \int_{v_{i-1}}^{v_i} \frac{de}{dt}(v)\frac{dt}{dv}\,dv \tag{44b}$$

$$\Theta_i^1 = \Theta_{i-1}^1 + \int_{v_{i-1}}^{v_i} \frac{d\Theta}{dt}(v)\frac{dt}{dv}\,dv \tag{44c}$$

where $dv/dt = na^2(1 - e^2)^{1/2}/r^2$.

The true anomaly v cannot be improved in this manner since an identity would naturally result. The true anomaly is adjusted by improved values of a and e. The process of Eqs. (44) would begin of course at the natural satellite measuring point where the orbital parameters of the spacecraft orbit are known.

The integrals on the right of Eqs. (44) are designated as

$$h_j(a,e,v,\Theta,J_2,J_4,C_{22},S_{22})|_{i-1}, \quad j = 1,2,3$$

which denote the difference between h_j evaluated with the parameters first solved at point i by Eqs. (19) and (25) and h_j evaluated with the parameters of point $i-1$. The h_j are listed in Ref. 6.

Nonplanetary Perturbations

The only significant nonplanetary contributions to $\dot{r}$ which must be removed before the solution of Eq. (13) are the perturbations caused by Jupiter's first five natural satellites—the four Galileans JI through JIV and Amalthea (JV). Orbital data for all five satellites are given in Table 1 (see Ref. 4). Since the orbital arc under consideration here has a short duration in the order of two hours, solar and other planetary perturbations can be neglected. The orbiter's distance and occultation from the sun during perijove crossing allows the elimination of solar radiation pressure as a perturbational cause. At a height of 7000 km from Jupiter's atmosphere of scale height 8.3 km, atmospheric drag is certainly no problem.[6] The irregular natural satellites JVI through JXII produce negligible perturbational effects as their distances to the spacecraft are very great while the spacecraft is in the measuring arc.

For the perturbational effects on $\dot{r}$ caused by the five satellites, the inclinations of the satellites can be ignored and the satellites' orbits are considered equatorial. This is justified by noting that the maximum inclination is 28.1 min of arc for Europa and that the inclination only affects the zenocentric angle between the spacecraft and the satellite, this angle being an argument of the Legendre polynomials developed below. The difference between this zenocentric angle and its projection into the equatorial plane is insignificant. The eccentricities must be kept general, however, even though they are quite small, because they vary the zenocentric ranges of the satellites by significant amounts.

The satellites' orbital parameters, substituted into Eq. (7), provide the corresponding zenocentric distances r_{ik} ($k = I, \ldots, V$) to the natural satellites k at any time t_i. The subscript i is now eliminated where it is understood that the development below is for each radar point.

The satellites' perturbational function (R) is well known in the n-body problem:

$$R = \sum_{k=1}^{5} GM_k \left(\frac{1}{\rho_k} - \frac{\mathbf{r}\cdot\mathbf{r}_k}{r_k^3} \right) \tag{45}$$

where G is the universal gravitational constant,[4] M_k is the mass of natural satellite k ($k = I, \ldots, V$), ρ_k is the distance between the spacecraft and satellite k, $\mathbf{r}$ is $\mathbf{r}_i$ or the zenocentric distance of the spacecraft, and $\mathbf{r}_k$ is $\mathbf{r}_{ik}$ or the zenocentric distance of satellite k at the ith observation point of the spacecraft. It is to be noted that generally there would not be a radar measurement to the satellite at this point and hence ρ_k is unknown but can be expressed as

$$\rho_k = (r^2 + r_k^2 - 2rr_k \cos\alpha)^{1/2} \tag{46}$$

$$\mathbf{r}\cdot\mathbf{r}_k = rr_k \cos\alpha \tag{47}$$

where α is the almost equatorial angle between r and r_k. It should be noted that the zenocentric distance r of the spacecraft during this arc of the orbit is always less than its value ($2.53\ R_J$) at true anomalies of $\pm\pi/2$, whereas all of the satellites are at distances greater than or equal to the closest satellite (Amalthea) at $2.54\ R_J$. Thus, during radar R and RR, $r < r_k, k = I, \ldots, V$. Then, for any term R_k of Eq. (45), using Eqs. (46) and (47):

$$R_k = \frac{GM_k}{r_k}\left[\left\{ 1 + \left(\frac{r}{r_k}\right)^2 - 2\left(\frac{r}{r_k}\right)\cos\alpha \right\}^{-1/2} - \left(\frac{r}{r_k}\right)\cos\alpha \right] \tag{48}$$

Equation (48) can be expressed as a series of Legendre polynomials and convergence is guaranteed by the fact that $r < r_k$. The first power of the series cancels the last term of Eq. (48) and there results

$$R_k = \frac{GM_k}{r_k} \sum_{\substack{m=0 \\ m\neq 1}}^{\infty} \left(\frac{r}{r_k}\right)^m P_m(\cos\alpha) \tag{49}$$

Looking at Fig. 6, it is seen that α is very nearly

$$\alpha = \Theta_k + v_k - (\Theta + v) \tag{50}$$

where Θ_k is approximately $\Omega_k + \omega_k$.

Thus R_k can now be expressed in terms of the spacecraft's orbital parameters:

$$R_k = \frac{GM_k}{r_k}\left\{ 1 + \sum_{m=2}^{\infty}\left[\frac{a(1-e^2)}{r_k(1+e\cos v)} \right]^m \times P_m[\cos\{\Theta_k + v_k - (\Theta + v)\}] \right\} \tag{51}$$

Substituting R_k for F in the Lagrange equations of equatorial perturbations Eq. (2) and then placing these orbital rates into the range rate model Eq. (12), much reduction finally yields

$$\dot{r}_k = \frac{GM_k(1-e^2)^{1/2}}{nar_k(1+e\cos v)} \sum_{m=2}^{\infty}\left(\frac{r}{r_k}\right)^m [H_1(e,v) \times P_{m1}[\cos\{\Theta_k + v_k - (\Theta + v)\}] - mH_2(v)P_m[\cos\{\Theta_k + v_k - (\Theta + v)\}]] \tag{52}$$

where $\dot{r}_k$ is the radial velocity of the spacecraft due to the perturbation of the kth natural satellite of Jupiter, n is the spacecraft mean orbital velocity, and

$$H_1(e,v) = (2 + e\cos v - 2\cos^2 v - e\cos^3 v)/(1 + e\cos v)$$

$$H_2(v) = \sin 2v$$

$P_{m1}(x)$ = Associated Legendre polynomial, degree m, order 1. r/r_k will usually be less than $\frac{1}{2}$, and the aforementioned infinite series will converge quickly and hence can be truncated after a few terms. Then the total range rate $\dot{r}'$ for each point i which must be subtracted from the measured range rate before substitution into equation Eq. (13) is

$$\dot{r}' = \sum_{k=1}^{5} \dot{r}_k \tag{53}$$

Conclusions

The formulation has been completely developed for deriving four harmonic coefficients of Jupiter's gravitational field by means of planetary radar measurements from a spacecraft having a highly eccentric orbit. The sequence of radar ranging takes advantage of onboard instruments during the short time interval that the spacecraft is within a few Jupiter radii of the planet's surface. Planetary range, range rate, and associated time of observation are required at each point along the orbit as well as one or more Amalthea radar measurements to provide an initial orbital set of parameters for at least one point. An alternative to the possibility of radar wave absorption in Jupiter's atmosphere would be the frequent radar measurements to Amalthea during the orbit about perijove. The undesirable feature of Amalthea measurements is the

changing of spacecraft attitude to point the radar antenna. These maneuvers might produce undesirable perturbations on the spacecraft which would mask the gravitational effects. Also satellite range and range rate would have to be reduced to an equivalent planetary range rate to apply the range rate model. This reduction involves errors in the ephemerides of the Jovian satellites.

The range rate model has been formulated in terms of the short term periodic perturbations on the spacecraft orbit due to Jupiter's gravitational potential. This model allows solution of four of Jupiter's gravitational harmonics. It should be remarked that the number of additional harmonics that might be added to the theory for solution depends not only on the value of the number of radar observations, but also on the instrumental accuracy obtainable in measuring range and range rate. It is meaningless to introduce additional higher degree gravitational harmonics into the range rate model the effects of which (on the spacecraft orbit) are less than the radar accuracy in measuring range rate. Rough calculations at a true anomaly of 20° for the spacecraft orbits considered here indicate that the J_2 term contributes about 600 m/sec and J_4 about 25 m/sec. Thus the J_4 contribution is quite close to the radar capability.

Judicial selection of the time intervals between successive radar measurements is desirable. From refined calculations near perijove and the radar accuracies mentioned earlier, it is deduced that the radar range and range rate measurements should all be performed within 17 sec at any measurement point, a time duration in which the planetary range and range rate vary by amounts detectable by the radar. Any successive planetary measurement of less than seventeen seconds would thus contribute no useful information; longer durations provide a greater difference between successive ranges which permits better definition of the Lambert condition for solving the orbital elements. Time intervals greater than one minute, however, would introduce errors in estimating the average semimajor axis between points.

A short-arc orbital determination scheme is developed solving the osculating orbital parameters at each radar measuring point. This is accomplished by first finding initial orbital values at a point where Amalthea radar measurements are obtained, and then progressing along the arc from point to point utilizing two orbital conditions involving each point.

If desired, an orbit refinement is possible after the first solution of the gravitational harmonic coefficients by the integration of the orbital rates of change between points.

Finally, the perturbations on the spacecraft due to Jupiter's first five natural satellites are formulated. To obtain some idea of the magnitudes of these perturbations, values were placed in Eq. (52) when the zenocentric longitudes of the spacecraft and a natural satellite were equal; i.e., $\Theta_k + v_k = \Theta + v$. It results that any natural satellite greater than 18.1 Jupiter radii perturbs the spacecraft's range rate by less than one meter per second, a rate below the estimated radar capability. Since the perturbation would be even less when nonalignment exists between the spacecraft and satellite, any satellite greater than 18.1 Jupiter radii can be eliminated from consideration; from Table 1, JIV (Callisto) will thus have no significant perturbations on the spacecraft.

References

[1] Kaula, W. M., *Theory of Satellite Geodesy*, Blaisdell, Waltham, Mass., 1966.

[2] *JOSÉ: A Jupiter Orbiting Spacecraft*, NASA Contract NGR 33-010-071, Cornell-NASA Research Group, 1971, under preparation.

[3] Michaux, C. M., *Handbook of the Physical Properties of the Planet Jupiter*, NASA SP-3031, 1967.

[4] Newburn, R. L., Jr., "A Brief Survey of the Major Planets: Jupiter, Saturn, Uranus, and Neptune," TM 33-424, April 1, 1969, Jet Propulsion Lab., Pasadena, Calif.

[5] Brouwer, D. and Clemence, G. M., "Orbits and Masses of Planets and Satellites," *The Solar System*, Vol. 3, The University of Chicago Press, Chicago, Ill., 1961, pp. 66, 72.

[6] Paul, C. K., *Attitude Control, Trajectory Analysis, and Science Objectives of a Jupiter Orbiting Spacecraft*, Ph.D. thesis, June 1970, Cornell Univ., Ithaca, N. Y.

[7] Brouwer, D. and Clemence, G. M., *Methods of Celestial Mechanics*, Academic Press, New York, 1961, pp. 273–308.